Title: Partitioning to ordered membrane domains regulates the kinetics of secretory traffic

Authors: Ivan Castello-Serrano[1], Fred A. Heberle[2], Barbara Diaz-Rohrer[3], Rossana Ippolito[1], Carolyn R. Shurer[1], Pablo Lujan[4], Felix Campelo[4], Kandice R. Levental[1*], Ilya Levental[1*]

Affiliations:

[1]Department of Molecular Physiology and Biological Physics, Center for Membrane and Cell Physiology, University of Virginia, Charlottesville, VA 22904

[2]Department of Chemistry, The University of Tennessee, Knoxville, TN 37996

[3]Broad Institute of MIT and Harvard

[4]ICFO-Institut de Ciencies Fotoniques, The Barcelona Institute of Science and Technology, Barcelona, Spain.

[*]corresponding authors: il2sy@virginia.edu , krl6c@virginia.edu

ABSTRACT

The organelles of eukaryotic cells maintain distinct protein and lipid compositions required for their specific functions. The mechanisms by which many of these components are sorted to their specific locations remain unknown. While some motifs mediating subcellular protein localization have been identified, many membrane proteins and most membrane lipids lack known sorting determinants. A putative mechanism for sorting of membrane components is based on membrane domains known as lipid rafts, which are laterally segregated nanoscopic assemblies of specific lipids and proteins. To assess the role of such domains in the secretory pathway, we applied a robust tool for synchronized secretory protein traffic (RUSH, Retention Using Selective Hooks) to protein constructs with defined affinity for raft phases. These constructs consist solely of single-pass transmembrane domains (TMDs) and, lacking other sorting determinants, constitute probes for membrane domain-mediated trafficking. We find that while raft affinity can be sufficient for steady-state PM localization, it is not sufficient for rapid exit from the endoplasmic reticulum (ER), which is instead mediated by a short cytosolic peptide motif. In contrast, we find that Golgi exit kinetics are highly dependent on raft affinity, with raft preferring probes exiting Golgi ~2.5-fold faster than probes with minimal raft affinity. We rationalize these observations with a kinetic model of secretory trafficking, wherein Golgi export can be facilitated by protein association with raft domains. These observations support a role for raft-like membrane domains in the secretory pathway and establish an experimental paradigm for dissecting its underlying machinery.

Introduction

Secretory and membrane proteins are synthesized in the endoplasmic reticulum (ER) followed by export of non-ER-resident proteins to the Golgi prior to sorting to their ultimate cellular location (Lippincott-Schwartz et al., 2000). Soluble and transmembrane proteins (TMPs) require somewhat different mechanisms to exit the ER, but both are dependent on the coat protein complex II (COPII), a multi-protein assembly recruited to the ER membrane to sort cargo and facilitate membrane deformation (Otte and Barlowe, 2004; Sato and Nakano, 2007). Cargo proteins are typically recognized for ER exit by binding

to COPII subunits via one of several short peptide motifs on their cytoplasmic tails (Barlowe, 2003a; Kuehn et al., 1998). Proteins that lack these motifs can be sorted by binding to motif-containing adaptors (Castillon et al., 2011; di Ronza et al., 2018). COPII mediated ER-to-Golgi transport is believed to proceed via vesicles (Gomez-Navarro et al., 2020; McCaughey and Stephens, 2019); however, recent observations suggest COPII mediates constrictions in continuous membrane structures connecting ER and Golgi membranes (Weigel et al., 2021).

The mechanisms and determinants of secretory and membrane protein sorting through the non-contiguous cisternae of the Golgi apparatus are less well understood. Non-resident proteins of the Golgi flux through distinct sub-compartments from cis-to-trans Golgi via several possible non-exclusive paths, including vesicles that exchange between static cisternae and/or dynamic cisternae that themselves change their composition and function over time (Lujan and Campelo, 2021; Pantazopoulou and Glick, 2019). Post-Golgi sorting generally occurs at the trans-Golgi network (TGN), where exiting proteins are packaged into transport carriers targeted to other organelles (Luini et al., 2008; Lujan et al., 2022; Nishimura et al., 2002; Tan and Gleeson, 2019). These sorting steps are at least partially mediated by clathrin (Ford et al., 2021) and its cargo-binding adapter proteins (Farias et al., 2012; Nishimura et al., 2002; Park and Guo, 2014). In some cases (e.g. mannose-6-phosphate), the principles of sorting are well understood (Puertollano et al., 2001). But for many other TMPs, the specific determinants of their subcellular trafficking itineraries and ultimate steady-state location are unknown. Even more mysterious are the rules for lipid sorting between various membranes, though lipid transfer machineries at membrane contact sites are likely important (Elbaz and Schuldiner, 2011; Mesmin et al., 2013; Phillips and Voeltz, 2016).

In parallel with polymerizing coats and motif-recognizing adapters, a putative scheme for sorting membrane lipids and proteins relies on nanodomains known as lipid rafts (Levental et al., 2020; Simons and Ikonen, 1997). Rafts arise due to the intrinsic capacity of biomembranes to laterally separate into coexisting ordered and disordered domains (Elson et al., 2010). Though still widely debated, recently accumulating evidence has validated many of the key predictions of the lipid raft hypothesis (Levental et al., 2020; Sezgin et al., 2017). One such predictions, indeed the original function for which lipid rafts were proposed, is that rafts facilitate polarized sorting in epithelial cells, assembling lipids and proteins for delivery from the trans-Golgi network to the apical PM (Lafont et al., 1999; Simons and Ikonen, 1997). Rafts have also been implicated in endocytic sorting (Gagescu et al., 2000), with some proteins relying on raft affinity for recycling to the PM after endocytosis (Diaz-Rohrer et al., 2023; Diaz-Rohrer et al., 2014b).

Key evidence supporting the capacity for biomembranes to form raft domains is provided by studies of plasma membranes isolated from living cells as Giant Plasma Membrane Vesicles (GPMVs). Such GPMVs separate into coexisting ordered and disordered phases that laterally sort membrane components according to their preference for certain membrane environments (Levental and Levental, 2015b). Namely, saturated lipids, glycolipids, GPI-anchored proteins, and selected TMPs co-enrich within a relatively tightly packed lipid phase (termed the "raft phase") (Sezgin et al., 2012), away from unsaturated phospholipids and most TMPs (Castello-Serrano et al., 2020; Levental et al., 2011). GPMVs thus provide a robust tool to quantitatively assess the intrinsic affinity of membrane components for raft-like domains

in biomembranes. Importantly, the preference of some TMPs for raft domains is tightly correlated with their subcellular localization, with raft association being necessary and sufficient for PM localization (Diaz-Rohrer et al., 2014b). For these, loss of raft affinity leads to accumulation in endo-lysosomes and ultimate degradation (Diaz-Rohrer et al., 2023).

While these observations, among many others (Abrami et al., 2003; Diaz-Rohrer et al., 2014a; Fabbri et al., 2005; Glebov et al., 2006; Sabharanjak et al., 2002), suggest that lipid-driven microdomains are involved in endocytosis and recycling, the role of rafts in the secretory pathway remains controversial and poorly understood due in large part to methodological limitations. Classical protocols for measuring raft association have been artifact-prone, non-quantitative, and difficult to interpret, while experiments relying on raft disruption are often pleiotropic (Levental et al., 2020; Munro, 2003). To circumvent these issues and directly interrogate the role of raft association in secretory traffic, we constructed a panel of minimal TMP probes with defined preferences for raft domains and measured their post-ER trafficking itineraries using RUSH, a robust tool for synchronized secretory traffic (Boncompain et al., 2012). We observed that raft association is sufficient for the steady-state distribution of some proteins, ER exit kinetics are largely determined by a sorting motif that likely mediates cargo association with COPII machinery. In contrast, raft affinity is sufficient to confer rapid efflux from the Golgi. We rationalize these observations with a kinetic model that generates a quantitative description of temporal transport of secretory cargo as a function of its association with various membrane subdomains. This model reproduces experimental observations and predicts separation of Golgi membranes into coexisting domains. Consistently, we microscopically observe separation of raft from non-raft probes in Golgi compartments and disruption of raft-associated Golgi efflux by inhibition of raft lipid synthesis. These observations reveal a role for lipid-driven domains in Golgi cargo sorting and provide a quantitative description of membrane protein dynamics through the secretory pathway.

Results

ER exit rates are determined more by cytosolic sorting motifs than raft affinity. In previous work, we used protein constructs comprised solely of transmembrane domains (TMDs) to interrogate raft-dependent recycling in the endocytic system (Diaz-Rohrer et al., 2023; Diaz-Rohrer et al., 2014b; Lorent et al., 2017). The preference of these probes for raft domains can be quantified directly by measuring their partitioning between ordered (raft) and disordered (non-raft) phases of isolated GPMVs (Levental and Levental, 2015a; Sezgin et al., 2012), as shown in Fig 1A-B. As previously shown (Diaz-Rohrer et al., 2014b; Lorent et al., 2017), the TMD of a single-pass transmembrane adapter called Linker for Activation of T-cells (LAT) preferentially partitions into the raft phase of GPMVs, away from the non-raft phase lipid marker (F-DiO) (Fig 1A, left). A model raft-excluded TMD is a 22-Leu construct (i.e. allL) which strongly prefers the non-raft phase (Fig 1A, right). This behavior can be quantified via the raft partition coefficient ($K_{p,raft}$) defined as the ratio of background-subtracted intensities for various constructs in the raft versus non-raft phases (Fig 1B). The LAT TMD (open symbols) retains the raft affinity of full-length LAT, while allL-TMD, either on its own or inserted into full-length LAT (LAT-allL), has very low raft affinity (Fig 1B).

To quantitatively assay the effects of raft affinity on the kinetics of secretory trafficking, we inserted these probes into the RUSH system, which allows synchronized release and tracking through the secretory system (Fig 1C). This assay is based on the reversible interaction of a target protein (fused to streptavidin-binding peptide, SBP) with a selective "hook"; e.g., streptavidin stably anchored in the ER via a KDEL motif. The strong interaction between the hook and SBP retains the protein of interest (POI) in the ER. Introduction of biotin causes rapid release of the POI, which is then tracked via a fluorescent tag. SBP-tagged versions (i.e. RUSH) of all constructs assayed here had indistinguishable raft affinity from non-SBP versions (RFP-only) (Fig 1B).

The isolated TMD of LAT was sufficient to recapitulate the steady-state plasma membrane (PM) localization of its full-length protein (Fig S1), consistent with previous reports (Diaz-Rohrer et al., 2014b; Lorent et al., 2017). In clear contrast, LAT-TMD did not recapitulate the ER exit kinetics of full-length LAT (Fig 1D). 45 mins after biotin addition, LAT had completely exited the ER and was localized almost exclusively to a bright perinuclear region, likely the Golgi. After 90 min, most full-length LAT achieved its steady-state localization at the PM. In contrast, LAT-TMD expressed in the same cell was still in the ER after 90 min and clearly accumulated at the PM only after several hours. Such slow kinetics were a challenge for live-cell imaging, so ER exit was quantified on a population level, by fixing cells at various time points after biotin addition and quantifying the fraction of cells with observable ER localization. The temporal reduction in the fraction of ER-positive cells was well described by a single-exponential fit for all constructs (e.g. Fig 1E), revealing that the half-time for ER exit was >4-fold faster for LAT (0.7 h) than for LAT-TMD (3.1 h) (Fig 1E-G).

We next tested whether raft affinity affected ER exit kinetics. To this end, we generated a RUSH construct of full-length LAT whose TMD was replaced with one that has minimal raft affinity (LAT-allL, Fig 1A). The general kinetics of ER exit of this non-raft LAT were comparable to LAT, with clear Golgi accumulation after 60 min of biotin. Post-Golgi accumulation was prominent at 90 min for both LAT and LAT-allL (the steady state localization of LAT-allL is in endolysosomes, Fig S1, as previously explained (Diaz-Rohrer et al., 2023; Diaz-Rohrer et al., 2014b)). In contrast, the isolated allL-TMD had much slower ER exit kinetics (Fig 1F-G). This trend was generalizable to several other proteins, with full-length versions having >3-fold faster ER exit kinetics than the TMD-only versions, regardless of their raft affinity (Fig 1F-G, Table S1). It is worth noting that isolated TMDs still exited the ER and reached a steady-state localization after several hours (Fig S1), despite no direct interactions with cytosolic trafficking machinery (e.g. COPII or clathrin). Altogether, we conclude that features present in cytosolic domains play a dominant role over TMD-determined raft affinity in ER exit.

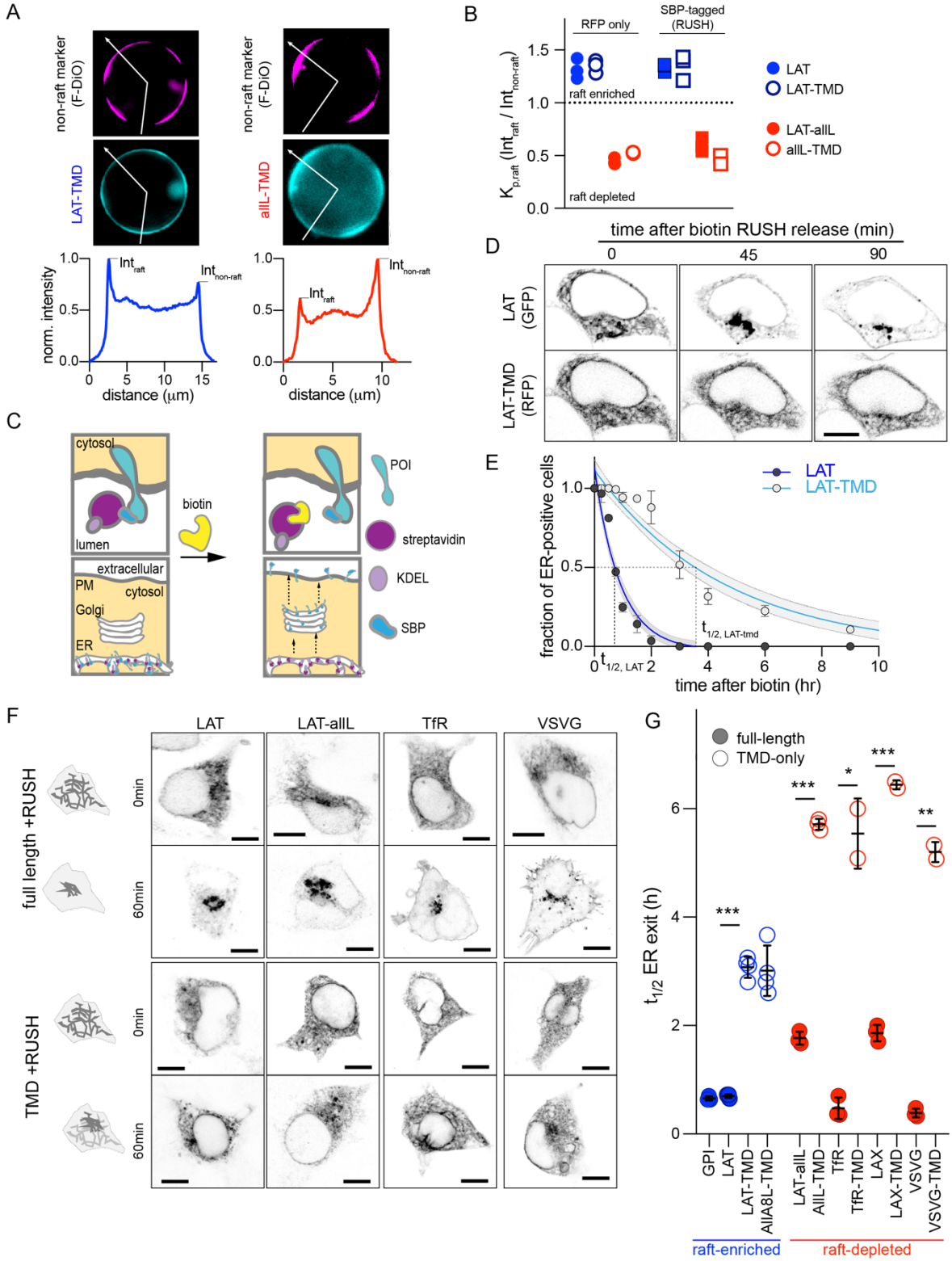

Figure 1. Full-length proteins exit the ER faster than TMD-only versions regardless of raft affinity. (A) Exemplary images of GPMVs from cells expressing raft-preferring LAT-TMD (left) or non-raft-preferring alIL-TMD (right). The RFP-tagged TMDs are shown in cyan; magenta shows the disordered phase marker Fast DiO (F-DiO). Bottom row shows fluorescence intensity line scans along white lines shown in cyan images, revealing protein partitioning between raft and non-raft phases. (B) The ratio of intensities in raft versus non-raft phase is the raft partition coefficient ($K_{p,raft}$). LAT-TMD and full-length LAT are enriched in the raft phase

while allL-TMD (and full-length LAT with allL-TMD, LAT-allL) are largely depleted from raft phase. SBP-tagging (for RUSH assay) has no effect on raft affinity. Symbols represent 3 independent experiments with >10 GPMVs/experiment. (C) Schematic of RUSH assay. (D) Confocal images of co-transfected LAT-EGFP and LAT-TMD-mRFP at various time points after biotin introduction. Full-length LAT exits ER faster. (E) Fraction of ER-positive cells decreases over time, allowing quantitative estimation of ER exit kinetics ($t_{1/2}$). Symbols represent average +/- st.dev. from >3 independent experiments. Fits represent exponential decays with shading representing 95% confidence intervals. (F) Confocal images of various full-length and TMD-only RUSH constructs (RFP-tagged) at 0 and 60 min after biotin introduction. (G) Quantification of $t_{1/2}$ for ER exit comparing full-length and TMD-only proteins (blue represents raft-enriched proteins, red = raft-depleted; see Table S1 for $K_{p,raft}$ quantifications). Bars represent average ± st.dev. from 3 independent experiments; *p<0.05, **p<0.01, ***p<0.001. All scale bars correspond to 5 μm.

LAT has a C-terminal ΦxΦxΦ ER exit motif. LAT is comprised of a minimal N-terminal ectodomain (<5 residues), a single-pass TMD, and a largely disordered cytosolic domain (CTD). Since LAT-TMD showed slow ER exit, we inferred that the determinant of rapid ER exit is likely located in the CTD and created a series of C-terminal truncations to locate the signal (Fig 2A). The two smaller C-term truncations (ΔCt1 and ΔCt2) had no effect on ER exit kinetics, behaving like full-length LAT (Fig 2B-C). In contrast, both larger truncations (ΔCt3 and ΔCt4) were significantly slower, behaving like LAT-TMD (Fig 2B-C). Thus, the motif facilitating fast ER exit of LAT is located within residues 140-185 (Fig 2A). We analyzed this fragment for possible COPII binding motifs (Barlowe, 2003b; Mikros and Diallinas, 2019) and identified ^{146}AAPSA^{152}, which corresponds to a ΦxΦxΦ motif (Φ = hydrophobic residue, x = spacer) (Otsu et al., 2013) (Fig 2A-inset). Point mutations in this putative motif confirmed that P148 and A150 were essential for fast ER exit, while other neighboring residues were not (Fig 2D-E and S2). We note that these two residues are highly conserved in LAT from 30 species (Fig 2A). Finally, inserting this AaPsA motif into LAT-TMD signficantly accelerated its ER exit, nearly recapitulating that of full-length LAT (Fig 2F). Thus, we conclude that fast ER exit of LAT is mediated by a ΦxΦxΦ motif in the cytosolic CTD, which likely mediates COPII association.

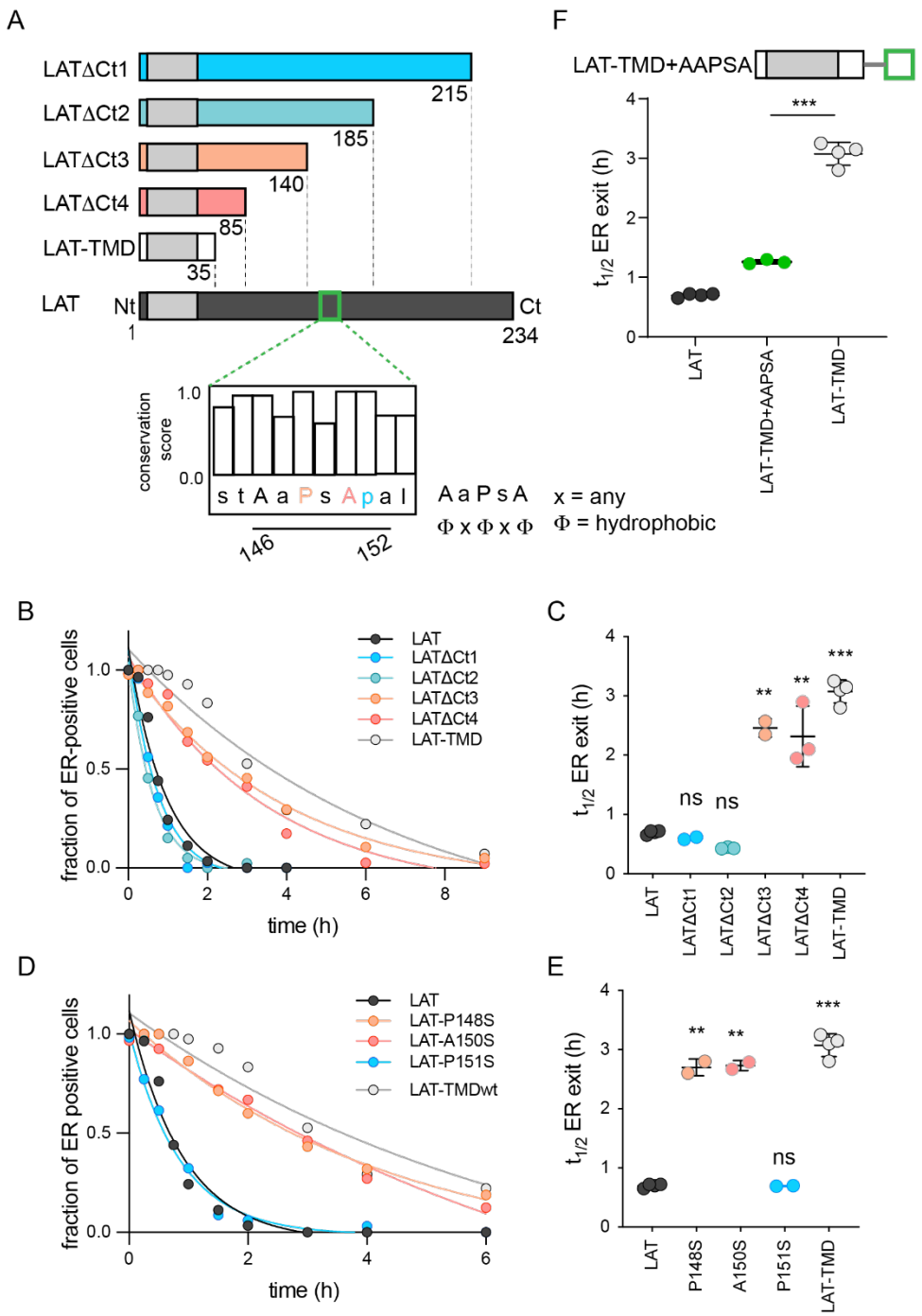

Figure 2. Identification of ER exit motif of LAT. (A) Schematic of LAT and the truncated versions used here. Inset shows a putative COPII association motif and the evolutionary conservation of residues 144-153 of hLAT. (B) Temporal dependence of the fraction of ER-positive cells for LAT truncations. Deletion of a region comprised of residues 140-185 leads to slow ER exit. (C) Fitted ER exit kinetics for the constructs represented in panel C. Deletion of amino acids 140-185 slows ER exit kinetics by ~4-fold. (D) Temporal dependence of fraction of ER-positive cells with point mutations of ΦxΦxΦ motif. Mutations of key residues within the motif slow ER exit kinetics. (E) Fitted ER exit kinetics for point mutants in panel D. (F) Insertion of AaPsA motif into LAT-TMD accelerates ER exit kinetics. B&D show a representative experiment with exponential decay fits; points in C,E, and F represent $t_{1/2}$ values of ER exit from fits of independent repeats with >20 cells/experiment. **p<0.01, ***p<0.001, ^{ns}p>0.05.

191 *Raft affinity determines Golgi exit kinetics of LAT.* The RUSH system can be adapted to measure exit rates
192 from Golgi by changing the "hook" to Golgin84, a resident protein of cis-Golgi (Diao et al., 2003). As
193 expected, all RUSH constructs (LAT, LAT-TMD, LAT-allL, allL-TMD) cotransfected with this hook
194 were localized almost exclusively in the Golgi without biotin (Fig 3A). Within 90 min of biotin
195 introduction, LAT exited the Golgi, achieving the expected steady-state PM localization (Fig 3A). LAT-
196 allL was clearly slower, with abundant Golgi signal remaining after 90 min. Tracking the kinetics by
197 quantitative imaging, LAT exited the Golgi ~2.5-fold faster than LAT-allL (Fig 3B-C). Strikingly, the
198 TMD-only versions of these constructs behaved nearly identically to the full-length (Fig 3B-C). LAT-
199 TMD, which has almost no residues that could interact with cytosolic trafficking machinery, had similar
200 Golgi-exit kinetics as full length VSVG (Fig S3), a model transmembrane secretory cargo. The kinetics
201 of VSVG traffic measured here with RUSH are consistent previous measurement by an orthogonal method
202 (Hirschberg et al., 1998), validating our approach.

203 To validate these conclusions in a different experimental paradigm, we measured Golgi exit kinetics after
204 a temperature block. It was previously shown that culturing mammalian cells at 15-20°C leads to
205 accumulation of secretory cargo in the Golgi (Milgram and Mains, 1994; Venditti et al., 2019). To
206 accumulate our probes in the Golgi, we used the ER-RUSH constructs to initially restrict them to the ER
207 (Fig 3D, left). Biotin was then added at 17°C for 3 h to release the protein from the ER and allow sufficient
208 time to accumulate in the Golgi. The cells were then shifted to 37°C to synchronize Golgi export. As with
209 Golgi-RUSH, LAT largely exited the Golgi within 90 min, whereas LAT-allL was significantly slower,
210 with notable Golgi accumulation remaining after 2 h (Fig 3D). The kinetics of the temperature-block
211 experiment were similar to Golgi RUSH, with raft-preferring LAT exiting Golgi ~2-fold faster than non-
212 raft LAT-allL. Based on these observations, we conclude that TMD-encoded raft affinity is an essential
213 determinant of Golgi exit kinetics for LAT.

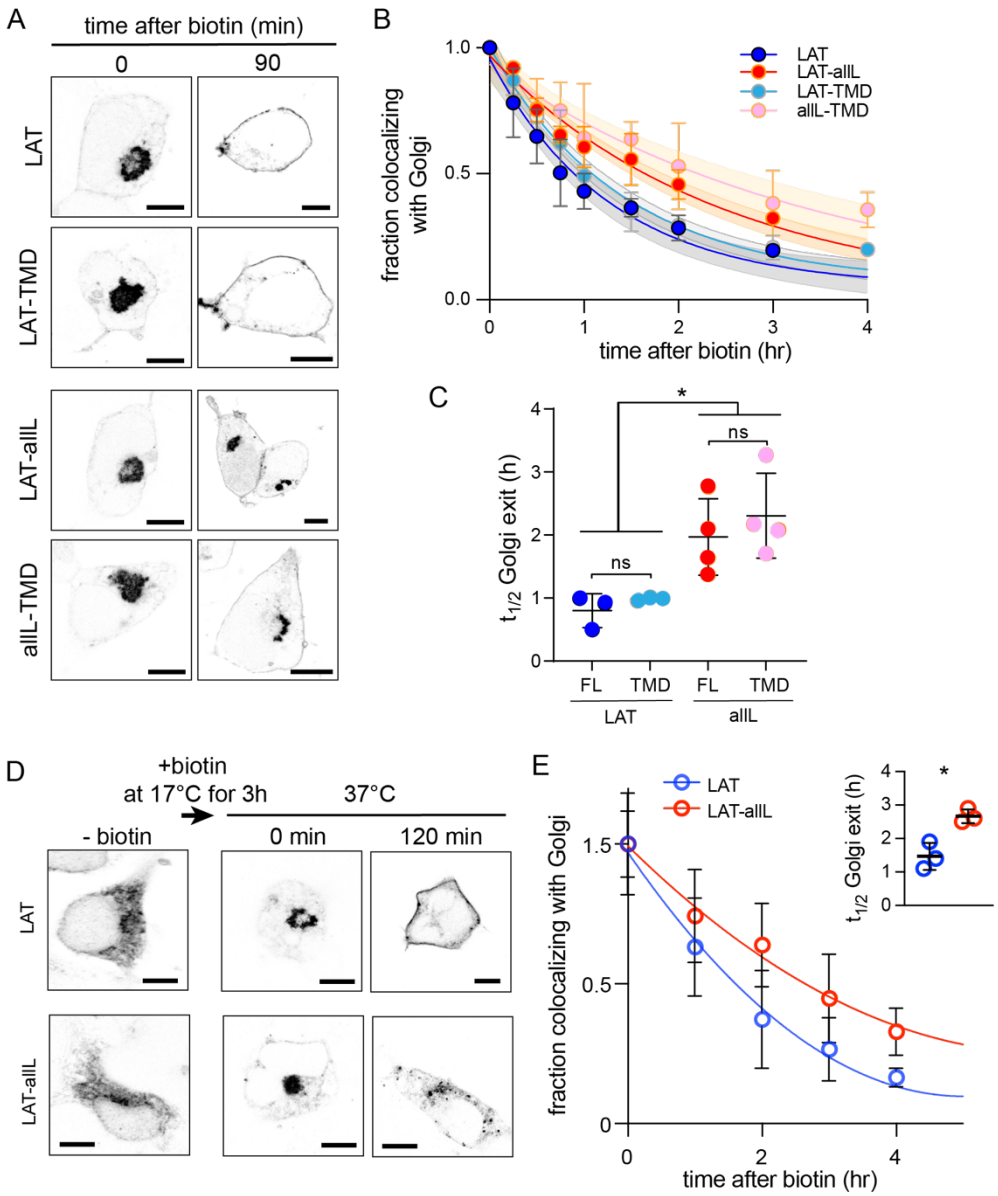

Figure 3. Golgi exit kinetics of LAT are dependent on its association with raft domains. (A) Representative confocal images of Golgi RUSH experiment show notable Golgi retention of non-raft constructs (LAT-allL and allL-TMD) after 90 min of biotin addition, in contrast to raft-preferring LAT and LAT-TMD. (B) Temporal reduction of protein constructs remaining in Golgi after biotin addition (i.e. release from Golgi RUSH), quantified by immunostaining and colocalization with Golgi marker (Giantin, see Fig S4). Symbols represent average +/- st.dev. from 3 independent experiments with >15 cells/experiment. Fits represent exponential decays; shading represents 95% confidence intervals. (C) Golgi exit rates for raft-associated LAT constructs are ~2.5-fold faster than non-raft versions for both full-length and TMD-only. Points represent $t_{1/2}$ values from fits of independent repeats with >20 cells/experiment. **$p<0.01$, $^{ns}p>0.05$. (D) Representative confocal images of full-length LAT and LAT-allL during Golgi temperature block. Addition of biotin at 17°C releases ER-RUSH constructs but traps them in Golgi. Removing temperature block by incubation at 37°C leads to fast PM trafficking of LAT but not non-raft LAT-allL. (E) Fraction of proteins in Golgi for the constructs shown in D, calculated as in B. Fits represent exponential decays. (inset) Golgi exit kinetics quantified as in C. All scale bars = 5 μm.

229 *Kinetic model of secretory traffic.* We attempted to rationalize our observations of ER and Golgi efflux
230 using a kinetic model wherein the secretory kinetics of a TMP are determined by equilibrium partitioning
231 between coexisting compartments in the ER and Golgi (Fig 4A). In the model, partitioning to an ER-exit
232 compartment (ERex) (analogous to a cellular ER exit site) allows ER efflux with first-order rate constant
233 k_a. Full-length and TMD-only proteins have different partition coefficients into this ERex compartment,
234 represented by two free fit parameters $K_{p,ERex_full}$ and $K_{p,ERex_TMD}$.

235 Analogously in the Golgi, we model coexisting compartments that enrich raft or non-raft proteins, again
236 with partition coefficients (i.e. $K_{p,raft_LAT}$ and $K_{p,raft_allL}$) describing the ratio of a protein's concentration in
237 the two compartments. These values were set by measurements of $K_{p,raft}$ for the various constructs in
238 GPMVs (Fig 1A-B), with the assumption that raft affinities measured at the PM are representative of those
239 in the Golgi. A first-order rate constant k_b is used to describe the transfer of proteins from the Golgi raft
240 sub-compartment to post-Golgi compartments. This conceptual model can be represented via a series of
241 coupled differential equations describing the temporal evolution of abundance of various constructs in
242 three compartments (ER, Golgi, post-Golgi). We emphasize that this model is highly simplified and does
243 not include many features relevant to trafficking of endogenous proteins. Rather, the goal was to identify
244 the minimal set of features that could describe the secretory behavior of our defined set of probes.

245 This simple model (four free parameters) was used to simultaneously fit experimental observations of
246 eight independent data sets, i.e. release from the ER or from the Golgi for four different protein constructs
247 (analogous to experiments described in Fig 1 and 3, respectively). For comparison to the models,
248 experimental datasets were re-measured via live-cell imaging (see Supp Fig 5) to directly quantify relative
249 construct abundance in the ER or Golgi. Model global fits nicely reproduced the general experimental
250 features of all constructs (Fig 4B), though with notable divergences. The general shape of both ER and
251 Golgi efflux curves were well described by the model and the specific Golgi efflux kinetics for all four
252 proteins were modeled quite accurately (Fig 4B, filled symbols). Consistent with expectation, the fitted
253 ER exit partition coefficient ($K_{p,ERex_full}$) for full-length constructs (i.e. those containing the putative COPII
254 binding motif) was ~20-fold greater than for TMD-only constructs. In contrast, the specific ER release
255 kinetics could not be completely reproduced, with the model underestimating ER efflux rate for both
256 constructs with raft-preferring TMDs, and overestimating those of the non-raft proteins (i.e. allL) (Fig.
257 4B, open symbols).

258 These fits could not be improved by adding a Golgi-to-ER retrieval path, consistent with none of our
259 constructs possessing a known retrieval motif (i.e. KDEL) (not shown). However, excellent agreement
260 between the model and all experimental observations could be obtained by allowing the ERex partition
261 coefficients of LAT and LAT-allL to independently vary (Fig 4C). Put another way, in this 5-parameter
262 fit, the TMD of these constructs was allowed to influence their affinity for the ER exit compartment. The
263 best-fit was obtained when LAT with a wild-type TMD had ~6-fold greater affinity for the ERex than
264 LAT-allL.

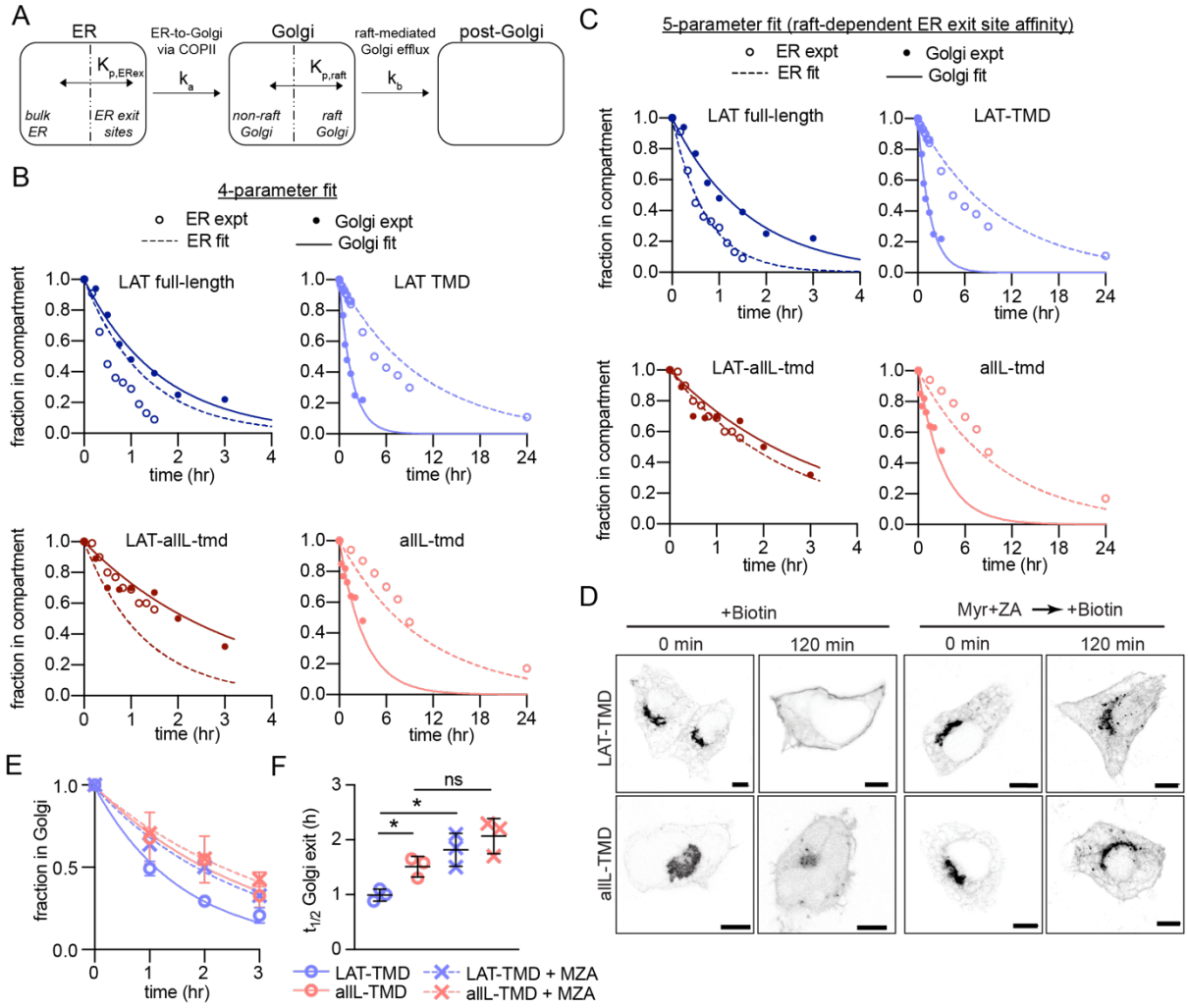

Figure 4. Kinetic model describing secretory traffic of LAT-based constructs. (A) Schematic of kinetic model. (B) Global fit of model with four free parameters to ER and Golgi RUSH data for four experimental constructs. (C) Global fit of model with five free parameters (different $K_{p,ERex}$ for LAT and LAT-allL). (D) Representative confocal images of Golgi RUSH experiments show notable Golgi retention for raft-preferring LAT after 2-day pre-treatment with Myr+ZA. Scale bars = 5 μm. (E) Temporal dependence of the fraction of protein constructs remaining in Golgi after biotin addition (to release from Golgi RUSH). Symbols represent average +/- st dev from 3 independent experiments with > 15 cells/exp. (F) Golgi exit rate for the raft-probe LAT-TMD is reduced when raft lipid synthesis is inhibited by Myr-ZA treatment. Points represent $t_{1/2}$ values of Golgi exit from fits of independent repeats with >20 cells/experiment. **p<0.01, ^{ns}p>0.05.

The general agreements between the model and observations support the plausibility of an underlying hypothesis that partitioning between coexisting membrane domains could explain the inter-organelle transfer kinetics in our study. A key aspect of the model is that selective Golgi membrane domains are important for Golgi exit kinetics of raft-associated cargo. To test this inference, we used inhibitors to block the production of raft-forming lipids (Lasserre et al., 2008; Levental et al., 2017) and tested their effects on trafficking rates of our probes. Specifically, sphingolipid and cholesterol synthesis were inhibited by treatment with 25 μM myriocin and 5 μM Zaragozic acid (MZA), respectively, for 2 days. This treatment was previously shown by us and others to reduce ordered membrane domain stability (Lasserre et al.,

283 2008; Levental et al., 2017; Wang et al., 2023). We observed significantly reduced Golgi exit kinetics of
284 LAT-TMD in MZA-treated cells, evidenced by clear Golgi localization up to 2 h after release of Golgi-
285 RUSH, in contrast to control cells (Fig 4D). Quantifying exit kinetics by imaging Golgi residence, we
286 observed that the half-time for Golgi exit was significantly increased (by ~60%) for the raft-preferring
287 TMD but not for the non-raft allL-TMD (Fig 4E-F).

288

289 *Segregation of raft from non-raft proteins in Golgi compartments.*

290 To directly image separation between raft and non-raft probes in the Golgi, we co-transfected RUSH
291 versions of LAT-TMD and allL-TMD with the Golgin84-hook to reversibly accumulate both constructs
292 in the Golgi. Their colocalization was then imaged using super-resolved Structured Illumination
293 Microscopy (SIM) (Fig 5A-B). Prior to introduction of biotin, the two constructs showed near-perfect
294 colocalization, as expected from their association with the same "hook". However, 5 minutes after
295 releasing the proteins with biotin, their colocalization was significantly reduced (Fig 5C), with areas of
296 LAT-TMD and allL-TMD enrichment apparent within the general morphology of the Golgi (Fig 5B).
297 Similar segregation of LAT-TMD from allL-TMD could be observed when both were accumulated in the
298 Golgi via a 20°C temperature block (Fig 5D). Notably, such segregation was not observed when LAT-
299 TMD was co-accumulated in the Golgi with either the full-length LAT or with raft-preferring GPI-GFP,
300 which colocalized nearly completely with each other (Fig 5D).

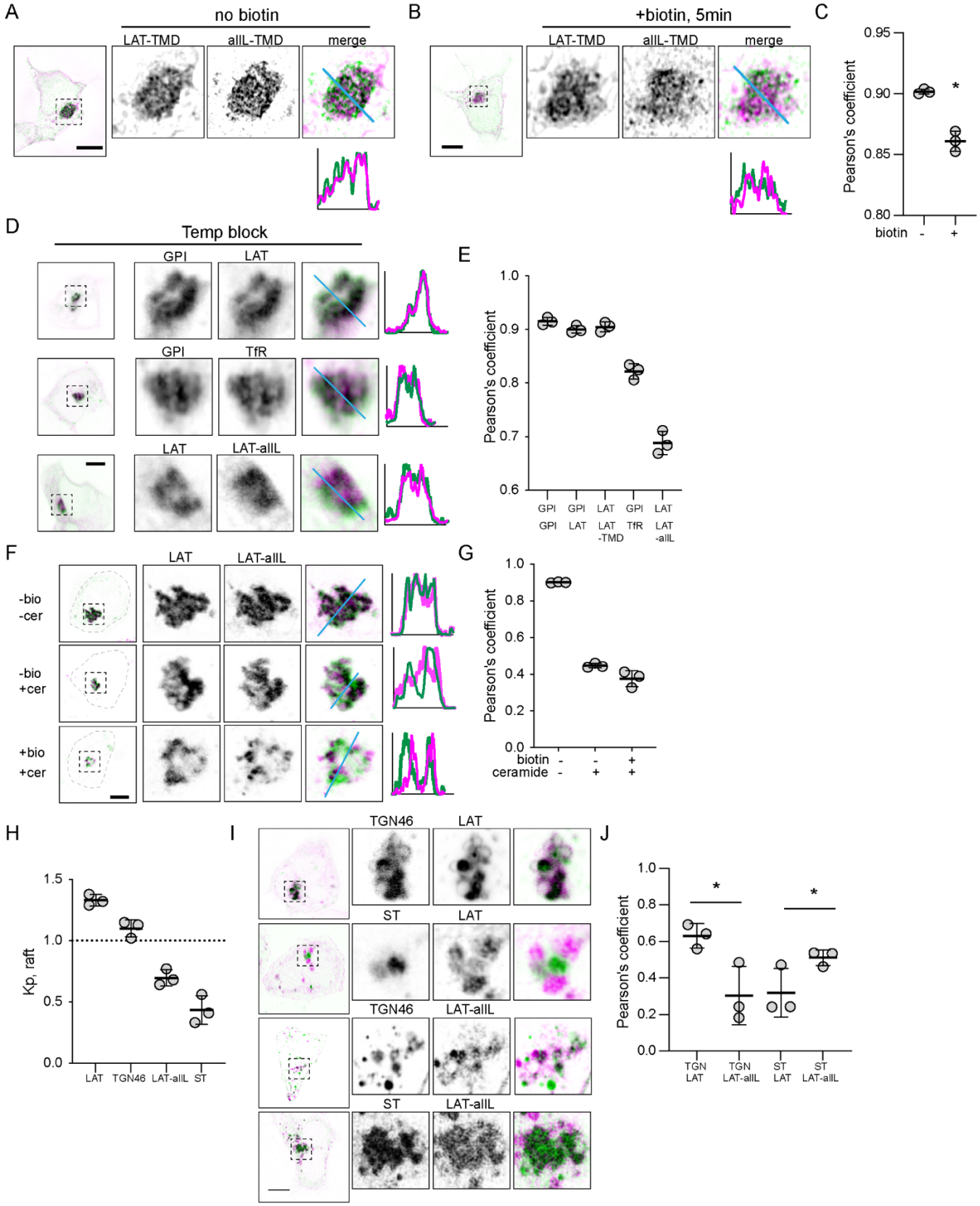

Figure 5. Raft probes segregate from non-raft in Golgi. (A) Raft vs non-raft probes trapped in Golgi by Golgi-RUSH (i.e. without biotin) and imaged by structured-illumination microscopy (SIM). (B) SIM images of localization of raft vs non-raft probes after 5 minutes of biotin addition to release Golgi RUSH. (C) Quantification of colocalization from SIM images by Pearson's coefficient in A and B. Symbols represent average +/- st. dev. from 3 independent

experiments with >15 cells/experiment. (D) Confocal images of cellular localization of co-transfected probes in cells grown at 20°C to accumulate probes in Golgi. (E) Quantification of colocalization under the conditions represented in D. (F) Images of cellular localization of co-transfected Golgi-RUSH probes after treatment with biotin or C6-Cer. (G) Quantification of colocalization under the conditions represented in F. (H) Quantification of raft affinity ($K_{p,raft}$) of TGN46 and ST, representatives of different Golgi sub-compartments. (I) Representative images of raft probes relative to Golgi sub-compartment markers under C6-Cer treatment. (J) Quantification of colocalization of proteins represented in I. Symbols in all quantifications are as in (A): average +/- st. dev. from 3 independent experiments with >15 cells/experiment. *p<0.05.

To support these observations without relying on temperature modulation, we treated cells with a short-chain Ceramide (D-Ceramide-C6, Cer-C6) which was previously reported to disrupt Golgi organization and post-Golgi transport (Capasso et al., 2017; Duran et al., 2012; van Galen et al., 2014). We combined this treatment with the Golgi-RUSH (Golgin84-hook) constructs to determine the fate of raft- and non-raft probes when their Golgi exit is blocked. Trapping both constructs in Golgi via RUSH produced very high co-localization, as expected (Fig 5F). When the constructs were released with biotin in cells treated with Cer-C6, LAT-TMD and allL-TMD both remained in a perinuclear compartment with the general morphology of the Golgi, but their colocalization was notably reduced, with raft-TMD-rich and -depleted areas visible under confocal imaging (Fig 5F). This reduced colocalization was also observed without biotin present, suggesting that Cer-C6 led to a remodeling of the Golgi and associated spatial segregation of raft from non-raft probe proteins, as previously proposed (van Galen et al., 2014).

These observations are consistent with previous reports that proteins can segregate in Golgi (Chen et al., 2017). Specifically, TGN46, a resident protein in the vesicular trans-Golgi network (TGN), was shown to physically segregate from a trans-Golgi-resident enzyme Sialyltransferase (ST) under Cer-C6 treatment (van Galen et al., 2014). To determine whether this physical segregation was related to the behavior of our raft domain probes, we co-transfected these Golgi-resident proteins with our probes and imaged them under Cer-C6 treatment. Intriguingly, in Cer-C6-treated cells, the raft probe (LAT-TMD) colocalized well with TGN46 but not with ST (Fig 5G-H). Conversely, the non-raft-preferring probe (allL-TMD) colocalized with ST, but not TGN46. These colocalization were consistent with the raft affinity of the Golgi markers evaluated in GPMVs: TGN46 was enriched in the raft phase approximately at parity with LAT-TMD, while ST was depleted from the raft phase (like allL-TMD). These observations support the hypothesis that proteins can segregate in Golgi based on their affinity for distinct membrane domains.

Discussion

The central paradigm of membrane protein traffic involves recognition of cargo sorting motifs by adaptor proteins, which then associate with coat-forming machinery to form inter-organelle trafficking intermediates with compositions that are distinct from their source organelles. Our study suggests that lipid-mediated organization also plays a supporting role in this process.

343 Several short motifs in cargo cytosolic domains have been reported to mediate recognition by the COPII
344 machinery for ER efflux. Originally identified were di-acidic (e.g. DxE) and di-Leu motifs (Barlowe,
345 2003b), and more recently other sequences with similar roles were identified (Barlowe, 2003b; Mikros
346 and Diallinas, 2019; Otsu et al., 2013). Our study reveals that a ΦxΦxΦ motif mediates fast ER exit of the
347 transmembrane scaffold LAT (Fig 2). Notably, constructs missing this motif (including LAT-TMD) still
348 eventually fully exit the ER and reach their steady-state localization, consistent with passive "leakage"
349 from the ER even in the absence of viable COPII interactions.

350 Although this motif plays a dominant role in determining LAT ER exit kinetics, our observations suggest
351 a minor contribution of lipid interactions with the protein's TMD. This contribution is revealed in different
352 ER exit kinetics of raft- and nonraft-preferring versions of either full-length or TMD-only constructs (Fig
353 1G). This inference was supported by the kinetic model, which showed the best global fit to experiments
354 when raft-preferring LAT-TMD had a somewhat higher partitioning to ER exit compartments than nonraft
355 LAT-allL (Fig 4C). A possible contribution of lipid domains to ER traffic is surprising, as ER cholesterol
356 abundance is believed to be too low to allow formation of ordered lipid domains (van Meer et al., 2008).
357 However, synthetic lipid experiments show that cholesterol concentrations as low as 10 mol% can support
358 liquid-ordered phases (Veatch and Keller, 2002, 2003) and locally high cholesterol concentrations are
359 possible through localized production, recruitment by proteins, and/or diffusion barriers (Prasad et al.,
360 2020). Indeed, enrichment of fluorescent cholesterol at some ER exit sites was recently reported (Weigel
361 et al., 2021). We emphasize that our study provides no direct evidence for rafts in the ER and much more
362 extensive characterization would be required to make a convincing claim. However, both our data and
363 model reveal that preferences of certain proteins for ordered membrane regions affect their ER exit rates.

364 Sorting of protein and lipid cargo in the Golgi is the originally proposed role for raft domains in cells
365 (Simons and Ikonen, 1997), supported by the Golgi's relatively high levels of cholesterol, sphingomyelin,
366 and glycolipids (Jackson et al., 2016; van Meer et al., 2008). Segregation of cargo prior to Golgi exit has
367 been microscopically observed (Chen et al., 2017) and anterograde sorting to the PM is facilitated by
368 palmitoylation (Chum et al., 2016; Ernst et al., 2018), a post-translational modification that imparts raft
369 affinity to many TMPs (Levental et al., 2010; Lorent et al., 2017). PM-directed vesicles in yeast are
370 enriched in sterols and sphingolipids relative to the Golgi, supporting a raft-based sorting model (Klemm
371 et al., 2009; Surma et al., 2011). Similarly, in mammalian cells, sphingomyelin is enriched in certain
372 Golgi-to-PM carriers (Deng et al., 2016; Sundberg et al., 2019). Our observations are fully consistent with
373 these results and implicate ordered lipid domains in LAT traffic from the Golgi. Full-length LAT and its
374 isolated TMD have similar Golgi efflux kinetics, both of which are approximately 2-fold faster than
375 nonraft analogs (Fig 3). This behavior was observed with either RUSH or temperature-block and
376 supported by our kinetic model, which predicts raft-dependent exit from the Golgi (Fig. 4). Whether these
377 observations reflect faster movement between cisternae or faster exit at the TGN remains an open question.

378 Direct visualization of lipid-driven domains remains a challenge, particularly acute in intracellular
379 membranes which are often small and have complex morphologies. Our SIM imaging suggests
380 segregation of raft from nonraft cargo in the Golgi shortly (5 min) after RUSH release (Fig 5B), but these

381 images only reveal reduced colocalization not actual protein distributions. Moreover, segregation within
382 a Golgi cisterna would be very difficult to distinguish from cargo moving between cisternae at different
383 rates or exiting via Golgi-proximal vesicles. Perhaps the most striking instance of separation of raft- from
384 nonraft-Golgi is observable after treatment with a short-chain ceramide (C6-cer), which has been reported
385 to disrupt formation of post-Golgi vesicles (Campelo et al., 2017; van Galen et al., 2014). In these distorted
386 Golgi, we observe selective colocalization of the raft probe with TGN-46, and *vice versa* for nonraft and
387 ST (Fig 6).

388 Collectively, these observations suggest that raft domains play a major role in Golgi-to-PM traffic for
389 certain cargoes and that raft affinity is the dominant determinant of Golgi efflux kinetics for LAT. This
390 protein belongs to a family of transmembrane adaptor proteins (TRAPs) with similar general structures
391 and functions (Chum et al., 2016; Park and Yun, 2009), suggesting that these observations may be relevant
392 for this class of proteins and perhaps others without motifs for clathrin- and adaptor-mediated sorting. In
393 contrast, rafts may play a more subordinate role in ER exit, perhaps facilitating the sorting of certain cargo
394 proteins and lipids to ER exit sites.

395

396 **Material and methods**

397 *Cell culture*

398 HEK-293NT (HEK) and HeLa cells were purchased from ATCC and cultured in medium containing 89%
399 Eagle's Minimum Essential Medium (EMEM), 10% FCS, and 1% penicillin/streptomycin at 37 °C in
400 humidified 5% CO2. COS-7 cells were cultured in medium containing the same formulation but with
401 Dulbecco Modified Essential Medium (DMEM) instead of EMEM and under the same conditions.
402 Transfection was done by Lipofectamine 3000 using the protocols provided with the reagents. 4–6 h after
403 transfection, cells were washed with PBS and then incubated with serum-free medium overnight. To
404 synchronize the cells, 1 h before biotin addition, the cells were given full-serum medium. Lipid synthesis
405 inhibitors (25 uM Myriocin and 5 uM Zaragozic Acid) were added for to the medium and given to the
406 cells 2 days before transfection and during the whole experiment. D-Ceramide-C6 was added to the
407 medium alone or in combination with biotin and given to the cells for 4 h, and then cells were fixed.

408 *Plasmids and mutations*

409 All single pass protein constructs from the ER were based on the bicistronic GPI RUSH backbone
410 previously described. We replaced the protein and fluorophore by the amino acid sequence of LAT-TMD,
411 which is NH2-MEEAILVPCVLGLLLLPILAMLMALCVHCHRLP followed by a short linker (GSGS)
412 and monomeric RFP (mRFP). A full length (LAT, LATallL, LAX) and TMD library (all-TMD, allA8L-
413 TMD, LAT-TMD6Dendo, TfR-TMD, LAX-TMD, VSVG-TMD, LATDC1-4, P148E, P148S, P148A,
414 A150S, P151S, P151A, A183S) were generated by amplifying the sequence of interest by PCR and
415 subsequent cloning of the mutant sequence into the LAT-TMD RUSH construct with KDEL hook to
416 synchronize from the ER. Several constructs were purchased from Addgene: full length RUSH version of
417 VSVG (#65300). All the single pass RUSH constructs from Golgi were based on the bicistronic VSVG

418 RUSH backbone kindly donated by Jennifer Lippincott-Schwartz lab. We cut the construct with BamHI
419 and EcoRI and replaced the protein with LAT, LATallL, LAT-TMD or all-TMD by amplifying the
420 sequence of interest by PCR. TGN46 and ST plasmids were provided by Felix Campelo lab.

421 *Imaging*

422 Unless specified, imaging was performed on a confocal microscope using appropriate filters for GFP/RFP
423 fluorescence for transfected plasmids. Single-cell tracking live imaging was performed using u-dish Grid-
424 50 glass bottom plates (Ibidi GmbH) to relocate the selected cells at each acquisition after incubating at
425 37°C in the incubator when not imaging. When needed, cells were fixed using 4% paraformaldehyde
426 (PFA), 10 min at RT. Anti-Giantin (1:1000 Rabbit polyclonal, Abcam ab80864) was used to create Golgi
427 mask.

428 *RUSH expression and chase*

429 In brief, transfected cells with different plasmids containing the RUSH retention system were incubated
430 overnight at 37 °C, and then incubated in the presence of 100 μM biotin (Sigma-Aldrich) to release the
431 cargo proteins. Cells were incubated at 37°C for various chase times and either directly imaged or fixed
432 with PFA as described above.

433 *GPMVs and Kp quants*

434 Cell membranes were stained with 5 μg/ml of FAST-DiO (Invitrogen), green fluorescent lipid dye that
435 strongly partitions to disordered phases(Levental and Levental, 2015b). Following staining, GPMVs were
436 isolated from transfected HEK-293, or HeLa cells as described (Sezgin et al., 2012)(cell type had no effect
437 on results). Briefly, GPMV formation was induced by 2 mM N-ethylmaleimide (NEM) in hypotonic
438 buffer containing 100 mM NaCl, 10 mM HEPES, and 2 mM CaCl2, pH 7.4. To quantify protein
439 partitioning, GPMVs were observed on an inverted epifluorescence microscope (Nikon) at 4°C after
440 treatment with 200 μM DCA to stabilize phase separation; this treatment has been previously
441 demonstrated not to affect raft affinity of various proteins (Zhou et al., 2013). The partition coefficient
442 ($K_{p,raft}$) for each protein construct was calculated from fluorescence intensity of the construct in the raft
443 and non-raft phase for >10 vesicles/trial (e.g. Fig. 1), with multiple independent experiments for each
444 construct.

445 *Conservation analysis*

446 After discarding uncharacterized proteins and taking just the first 100 results from 246 hits in the Blast
447 for LAT sequence extracted from Uniprot database, we have used Unipro Ugene to analyze the results of
448 30 species with > 80% similarity.

449 *Kinetic model for trafficking of RUSH constructs.* Residence fraction data were analyzed globally by
450 numerically solving a first-order, homogeneous system of equations that accounts for intra- and inter-
451 compartment transport. A schematic of the trafficking model is shown in Fig. 4A. Briefly, the ER was
452 modeled with two sub-compartments representing bulk and exit sites, with an intra-ER partition
453 coefficient $K_{p,ERex}$, defined as the ratio of concentrations between the exit and bulk compartments.

Similarly, the Golgi was modeled with two sub-compartments representing raft and non-raft sites, with an intra-Golgi partition coefficient $K_{p,raft}$,, i.e. the ratio of concentrations between the raft and nonraft compartments. These values are set in the model via measurements of $K_{p,raft}$ in GPMVs (Fig 1)(Diaz-Rohrer et al., 2023; Lorent et al., 2017). Inter-compartment trafficking from ER to Golgi initiates from ER exit sites and terminates at the Golgi with a rate constant k_a, while unidirectional post-Golgi traffic originating from Golgi raft sites was modeled with a rate constant k_b. In total, the trafficking model for a given construct is a function of two rate constants and two partition coefficients, one of which is fixed experimentally.

Eight data sets representing the ER and Golgi efflux kinetics of LAT, LAT-TMD, AllL-LAT, and AllL-TMD were fit to the trafficking model. We performed a single global analysis (i.e. simultaneous fit of all eight data sets) using k_a, k_b, and two $K_{p,ERex}$ (one for full-length and one for TMD-only) as free fit parameters. A second analysis included a third $K_{p,ERex}$, allowing LAT and LAT-allL to be different.

All analysis was performed with custom code written in Mathematica v.12.2 (Wolfram Research Inc., Champaign, IL). Model parameters were optimized with a Levenberg-Marquardt algorithm implemented in the built-in Mathematica function NonlinearModelFit. The target function for minimization was the sum of squared residuals for the combined data sets, $\chi^2 = \sum_i \sum_j (y_{ij} - \bar{y}_{ij})^2$, where i indexes the eight data sets, j indexes the data points within a data set, y_{ij} is the observed residence fraction, and $\bar{y}_{ij}$ is the predicted residence fraction. To improve the probability of finding the global minimum, the optimization was repeated 10^3 times with different random initial values for the adjustable parameters; the best-fit parameters associated with the overall lowest χ^2 value is reported as the solution.

Acknowledgements

We thank members of the Levental lab for their discussions and critical feedback. Funding for this work was provided by the NIH/National Institute of General Medical Sciences (GM124072, GM134949, F32GM145028 to CRS), the Volkswagen Foundation (grant 93091), and the Human Frontiers Science Program (RGP0059/2019). Flow cytometry was performed in the University of Virginia Flow Cytometry Core, RRID: SCR_017829. All authors have no competing interests. The order of equally contributing authors is arbitrary. P.L. and F.C. acknowledge support from the Government of Spain (RYC-2017-22227, PID2019-106232RB-I00/10.13039/501100011033; Severo Ochoa CEX2019-000910-S), Fundació Cellex, Fundació Mir-Puig, and Generalitat de Catalunya (CERCA, AGAUR).

References

Abrami, L., Liu, S., Cosson, P., Leppla, S.H., and van der Goot, F.G. (2003). Anthrax toxin triggers endocytosis of its receptor via a lipid raft-mediated clathrin-dependent process. J Cell Biol *160*, 321-328.

Barlowe, C. (2003a). Molecular recognition of cargo by the COPII complex: a most accommodating coat. Cell *114*, 395-397.

490 Barlowe, C. (2003b). Signals for COPII-dependent export from the ER: what's the ticket out? Trends in cell biology
491 *13*, 295-300.
492 Boncompain, G., Divoux, S., Gareil, N., de Forges, H., Lescure, A., Latreche, L., Mercanti, V., Jollivet, F., Raposo, G.,
493 and Perez, F. (2012). Synchronization of secretory protein traffic in populations of cells. Nat Methods *9*, 493-498.
494 Campelo, F., van Galen, J., Turacchio, G., Parashuraman, S., Kozlov, M.M., Garcia-Parajo, M.F., and Malhotra, V.
495 (2017). Sphingomyelin metabolism controls the shape and function of the Golgi cisternae. eLife *6*.
496 Capasso, S., Sticco, L., Rizzo, R., Pirozzi, M., Russo, D., Dathan, N.A., Campelo, F., van Galen, J., Holtta-Vuori, M.,
497 Turacchio, G*., et al.* (2017). Sphingolipid metabolic flow controls phosphoinositide turnover at the trans-Golgi
498 network. EMBO J *36*, 1736-1754.
499 Castello-Serrano, I., Lorent, J.H., Ippolito, R., Levental, K.R., and Levental, I. (2020). Myelin-Associated MAL and
500 PLP Are unusual among multipass transmembrane proteins in preferring ordered membrane domains. J Phys
501 Chem B *124*, 5930-5939.
502 Castillon, G.A., Aguilera-Romero, A., Manzano-Lopez, J., Epstein, S., Kajiwara, K., Funato, K., Watanabe, R.,
503 Riezman, H., and Muniz, M. (2011). The yeast p24 complex regulates GPI-anchored protein transport and quality
504 control by monitoring anchor remodeling. Mol Biol Cell *22*, 2924-2936.
505 Chen, Y., Gershlick, D.C., Park, S.Y., and Bonifacino, J.S. (2017). Segregation in the Golgi complex precedes export
506 of endolysosomal proteins in distinct transport carriers. J Cell Biol *216*, 4141-4151.
507 Chum, T., Glatzova, D., Kvicalova, Z., Malinsky, J., Brdicka, T., and Cebecauer, M. (2016). The role of palmitoylation
508 and transmembrane domain in sorting of transmembrane adaptor proteins. J Cell Sci *129*, 95-107.
509 Deng, Y., Rivera-Molina, F.E., Toomre, D.K., and Burd, C.G. (2016). Sphingomyelin is sorted at the trans Golgi
510 network into a distinct class of secretory vesicle. Proc Natl Acad Sci U S A *113*, 6677-6682.
511 di Ronza, A., Bajaj, L., Sharma, J., Sanagasetti, D., Lotfi, P., Adamski, C.J., Collette, J., Palmieri, M., Amawi, A., Popp,
512 L*., et al.* (2018). CLN8 is an endoplasmic reticulum cargo receptor that regulates lysosome biogenesis. Nat Cell Biol
513 *20*, 1370-1377.
514 Diao, A., Rahman, D., Pappin, D.J., Lucocq, J., and Lowe, M. (2003). The coiled-coil membrane protein golgin-84 is
515 a novel rab effector required for Golgi ribbon formation. J Cell Biol *160*, 201-212.
516 Diaz-Rohrer, B., Castello-Serrano, I., Chan, S.H., Wang, H., Shurer, C.R., Levental, K.R., and Levental, I. (2023). Rab3
517 mediates a pathway for endocytic sorting and plasma membrane recycling of ordered microdomains Proc Natl
518 Acad Sci U S A *in press*.
519 Diaz-Rohrer, B., Levental, K.R., and Levental, I. (2014a). Rafting through traffic: Membrane domains in cellular
520 logistics. Biochim Biophys Acta-Biomembr *1838*, 3003-3013.
521 Diaz-Rohrer, B.B., Levental, K.R., Simons, K., and Levental, I. (2014b). Membrane raft association is a determinant
522 of plasma membrane localization. Proc Natl Acad Sci U S A *111*, 8500-8505.
523 Duran, J.M., Campelo, F., van Galen, J., Sachsenheimer, T., Sot, J., Egorov, M.V., Rentero, C., Enrich, C., Polishchuk,
524 R.S., Goni, F.M*., et al.* (2012). Sphingomyelin organization is required for vesicle biogenesis at the Golgi complex.
525 EMBO J *31*, 4535-4546.
526 Elbaz, Y., and Schuldiner, M. (2011). Staying in touch: the molecular era of organelle contact sites. Trends Biochem
527 Sci *36*, 616-623.
528 Elson, E.L., Fried, E., Dolbow, J.E., and Genin, G.M. (2010). Phase separation in biological membranes: integration
529 of theory and experiment. Annu Rev Biophys *39*, 207-226.
530 Ernst, A.M., Syed, S.A., Zaki, O., Bottanelli, F., Zheng, H., Hacke, M., Xi, Z., Rivera-Molina, F., Graham, M., Rebane,
531 A.A*., et al.* (2018). S-Palmitoylation Sorts Membrane Cargo for Anterograde Transport in the Golgi. Dev Cell *47*,
532 479-493 e477.
533 Fabbri, M., Di Meglio, S., Gagliani, M.C., Consonni, E., Molteni, R., Bender, J.R., Tacchetti, C., and Pardi, R. (2005).
534 Dynamic partitioning into lipid rafts controls the endo-exocytic cycle of the alphaL/beta2 integrin, LFA-1, during
535 leukocyte chemotaxis. Mol Biol Cell *16*, 5793-5803.
536 Farias, G.G., Cuitino, L., Guo, X., Ren, X., Jarnik, M., Mattera, R., and Bonifacino, J.S. (2012). Signal-mediated, AP-
537 1/clathrin-dependent sorting of transmembrane receptors to the somatodendritic domain of hippocampal
538 neurons. Neuron *75*, 810-823.
539 Ford, C., Parchure, A., von Blume, J., and Burd, C.G. (2021). Cargo sorting at the trans-Golgi network at a glance.
540 Journal of Cell Science *134*.

541 Gagescu, R., Demaurex, N., Parton, R.G., Hunziker, W., Huber, L.A., and Gruenberg, J. (2000). The recycling
542 endosome of Madin-Darby canine kidney cells is a mildly acidic compartment rich in raft components. Mol Biol
543 Cell *11*, 2775-2791.
544 Glebov, O.O., Bright, N.A., and Nichols, B.J. (2006). Flotillin-1 defines a clathrin-independent endocytic pathway in
545 mammalian cells. Nat Cell Biol *8*, 46-54.
546 Gomez-Navarro, N., Melero, A., Li, X.H., Boulanger, J., Kukulski, W., and Miller, E.A. (2020). Cargo crowding
547 contributes to sorting stringency in COPII vesicles. J Cell Biol *219*.
548 Hirschberg, K., Miller, C.M., Ellenberg, J., Presley, J.F., Siggia, E.D., Phair, R.D., and Lippincott-Schwartz, J. (1998).
549 Kinetic analysis of secretory protein traffic and characterization of golgi to plasma membrane transport
550 intermediates in living cells. J Cell Biol *143*, 1485-1503.
551 Jackson, C.L., Walch, L., and Verbavatz, J.M. (2016). Lipids and Their Trafficking: An Integral Part of Cellular
552 Organization. Dev Cell *39*, 139-153.
553 Klemm, R.W., Ejsing, C.S., Surma, M.A., Kaiser, H.J., Gerl, M.J., Sampaio, J.L., de Robillard, Q., Ferguson, C.,
554 Proszynski, T.J., Shevchenko, A*., et al.* (2009). Segregation of sphingolipids and sterols during formation of
555 secretory vesicles at the trans-Golgi network. J Cell Biol *185*, 601-612.
556 Kuehn, M.J., Herrmann, J.M., and Schekman, R. (1998). COPII-cargo interactions direct protein sorting into ER-
557 derived transport vesicles. Nature *391*, 187-190.
558 Lafont, F., Verkade, P., Galli, T., Wimmer, C., Louvard, D., and Simons, K. (1999). Raft association of SNAP receptors
559 acting in apical trafficking in Madin–Darby canine kidney cells. Proceedings of the National Academy of
560 Sciences *96*, 3734-3738.
561 Lasserre, R., Guo, X.J., Conchonaud, F., Hamon, Y., Hawchar, O., Bernard, A.M., Soudja, S.M., Lenne, P.F., Rigneault,
562 H., Olive, D*., et al.* (2008). Raft nanodomains contribute to Akt/PKB plasma membrane recruitment and activation.
563 Nat Chem Biol *4*, 538-547.
564 Levental, I., Grzybek, M., and Simons, K. (2011). Raft domains of variable properties and compositions in plasma
565 membrane vesicles. Proceedings of the National Academy of Sciences *108*, 11411-11416.
566 Levental, I., Levental, K.R., and Heberle, F.A. (2020). Lipid rafts: controversies resolved, mysteries remain. Trends
567 in cell biology *30*, 341-353.
568 Levental, I., Lingwood, D., Grzybek, M., Coskun, U., and Simons, K. (2010). Palmitoylation regulates raft affinity for
569 the majority of integral raft proteins. Proc Natl Acad Sci U S A *107*, 22050-22054.
570 Levental, K.R., and Levental, I. (2015a). Giant plasma membrane vesicles: models for understanding membrane
571 organization. Current topics in membranes *75*, 25-57.
572 Levental, K.R., and Levental, I. (2015b). Isolation of giant plasma membrane vesicles for evaluation of plasma
573 membrane structure and protein partitioning. Methods in molecular biology *1232*, 65-77.
574 Levental, K.R., Surma, M.A., Skinkle, A.D., Lorent, J.H., Zhou, Y., Klose, C., Chang, J.T., Hancock, J.F., and Levental,
575 I. (2017). omega-3 polyunsaturated fatty acids direct differentiation of the membrane phenotype in mesenchymal
576 stem cells to potentiate osteogenesis. Science advances *3*, eaao1193.
577 Lippincott-Schwartz, J., Roberts, T.H., and Hirschberg, K. (2000). Secretory protein trafficking and organelle
578 dynamics in living cells. Annu Rev Cell Dev Biol *16*, 557-589.
579 Lorent, J.H., Diaz-Rohrer, B., Lin, X., Spring, K., Gorfe, A.A., Levental, K.R., and Levental, I. (2017). Structural
580 determinants and functional consequences of protein affinity for membrane rafts. Nature communications *8*,
581 1219.
582 Luini, A., Mironov, A.A., Polishchuk, E.V., and Polishchuk, R.S. (2008). Morphogenesis of post-Golgi transport
583 carriers. Histochem Cell Biol *129*, 153-161.
584 Lujan, P., and Campelo, F. (2021). Should I stay or should I go? Golgi membrane spatial organization for protein
585 sorting and retention. Archives of biochemistry and biophysics *707*, 108921.
586 Lujan, P., Garcia-Cabau, C., Wakana, Y., Rodilla-Ramírez, C., Malhotra, V., Salvatella, X., Garcia-Parajo, M.F., and
587 Campelo, F. (2022). Sorting of secretory proteins at the trans-Golgi network by TGN46. bioRxiv,
588 2022.2004.2020.488883.
589 McCaughey, J., and Stephens, D.J. (2019). ER-to-Golgi Transport: A Sizeable Problem. Trends Cell Biol *29*, 940-953.
590 Mesmin, B., Bigay, J., Moser von Filseck, J., Lacas-Gervais, S., Drin, G., and Antonny, B. (2013). A four-step cycle
591 driven by PI(4)P hydrolysis directs sterol/PI(4)P exchange by the ER-Golgi tether OSBP. Cell *155*, 830-843.

592 Mikros, E., and Diallinas, G. (2019). Tales of tails in transporters. Open Biol *9*, 190083.
593 Milgram, S.L., and Mains, R.E. (1994). Differential effects of temperature blockade on the proteolytic processing
594 of three secretory granule-associated proteins. J Cell Sci *107 (Pt 3)*, 737-745.
595 Munro, S. (2003). Lipid rafts: elusive or illusive? Cell *115*, 377-388.
596 Nishimura, N., Plutner, H., Hahn, K., and Balch, W.E. (2002). The delta subunit of AP-3 is required for efficient
597 transport of VSV-G from the trans-Golgi network to the cell surface. Proc Natl Acad Sci U S A *99*, 6755-6760.
598 Otsu, W., Kurooka, T., Otsuka, Y., Sato, K., and Inaba, M. (2013). A new class of endoplasmic reticulum export
599 signal PhiXPhiXPhi for transmembrane proteins and its selective interaction with Sec24C. J Biol Chem *288*, 18521-
600 18532.
601 Otte, S., and Barlowe, C. (2004). Sorting signals can direct receptor-mediated export of soluble proteins into COPII
602 vesicles. Nat Cell Biol *6*, 1189-1194.
603 Pantazopoulou, A., and Glick, B.S. (2019). A Kinetic View of Membrane Traffic Pathways Can Transcend the
604 Classical View of Golgi Compartments. Frontiers in cell and developmental biology *7*, 153.
605 Park, I., and Yun, Y. (2009). Transmembrane adaptor proteins positively regulating the activation of lymphocytes.
606 Immune Netw *9*, 53-57.
607 Park, S.Y., and Guo, X. (2014). Adaptor protein complexes and intracellular transport. Biosci Rep *34*.
608 Phillips, M.J., and Voeltz, G.K. (2016). Structure and function of ER membrane contact sites with other organelles.
609 Nat Rev Mol Cell Biol *17*, 69-82.
610 Prasad, R., Sliwa-Gonzalez, A., and Barral, Y. (2020). Mapping bilayer thickness in the ER membrane. Science
611 advances *6*.
612 Puertollano, R., Aguilar, R.C., Gorshkova, I., Crouch, R.J., and Bonifacino, J.S. (2001). Sorting of Mannose 6-
613 Phosphate Receptors Mediated by the GGAs. Science *292*, 1712-1716.
614 Sabharanjak, S., Sharma, P., Parton, R.G., and Mayor, S. (2002). GPI-anchored proteins are delivered to recycling
615 endosomes via a distinct cdc42-regulated, clathrin-independent pinocytic pathway. Dev Cell *2*, 411-423.
616 Sato, K., and Nakano, A. (2007). Mechanisms of COPII vesicle formation and protein sorting. FEBS Lett *581*, 2076-
617 2082.
618 Sezgin, E., Kaiser, H.J., Baumgart, T., Schwille, P., Simons, K., and Levental, I. (2012). Elucidating membrane
619 structure and protein behavior using giant plasma membrane vesicles. Nat Protoc *7*, 1042-1051.
620 Sezgin, E., Levental, I., Mayor, S., and Eggeling, C. (2017). The mystery of membrane organization: composition,
621 regulation and roles of lipid rafts. Nat Rev Mol Cell Biol *18*, 361-374.
622 Simons, K., and Ikonen, E. (1997). Functional rafts in cell membranes. Nature *387*, 569-572.
623 Sundberg, E.L., Deng, Y., and Burd, C.G. (2019). Syndecan-1 Mediates Sorting of Soluble Lipoprotein Lipase with
624 Sphingomyelin-Rich Membrane in the Golgi Apparatus. Dev Cell.
625 Surma, M.A., Klose, C., Klemm, R.W., Ejsing, C.S., and Simons, K. (2011). Generic sorting of raft lipids into secretory
626 vesicles in yeast. Traffic *12*, 1139-1147.
627 Tan, J.Z.A., and Gleeson, P.A. (2019). Cargo Sorting at the trans-Golgi Network for Shunting into Specific Transport
628 Routes: Role of Arf Small G Proteins and Adaptor Complexes. Cells *8*.
629 van Galen, J., Campelo, F., Martinez-Alonso, E., Scarpa, M., Martinez-Menarguez, J.A., and Malhotra, V. (2014).
630 Sphingomyelin homeostasis is required to form functional enzymatic domains at the trans-Golgi network. J Cell
631 Biol *206*, 609-618.
632 van Meer, G., Voelker, D.R., and Feigenson, G.W. (2008). Membrane lipids: where they are and how they behave.
633 Nat Rev Mol Cell Biol *9*, 112-124.
634 Veatch, S.L., and Keller, S.L. (2002). Organization in lipid membranes containing cholesterol. Phys Rev Lett *89*,
635 268101.
636 Veatch, S.L., and Keller, S.L. (2003). Separation of liquid phases in giant vesicles of ternary mixtures of
637 phospholipids and cholesterol. Biophys J *85*, 3074-3083.
638 Venditti, R., Masone, M.C., Rega, L.R., Di Tullio, G., Santoro, M., Polishchuk, E., Serrano, I.C., Olkkonen, V.M.,
639 Harada, A., Medina, D.L*., et al.* (2019). The activity of Sac1 across ER-TGN contact sites requires the four-
640 phosphate-adaptor-protein-1. J Cell Biol *218*, 783-797.

641 Wang, H., Chan, S.H., Dey, S., Castello-Serrano, I., Ditlev, J.A., Rosen, M.K., Levental, K.R., and Levental, I. (2023).
642 Coupling of protein condensates to ordered lipid domains determines functional membrane organization. Science
643 advances *in press*.
644 Weigel, A.V., Chang, C.L., Shtengel, G., Xu, C.S., Hoffman, D.P., Freeman, M., Iyer, N., Aaron, J., Khuon, S., Bogovic,
645 J.*, et al.* (2021). ER-to-Golgi protein delivery through an interwoven, tubular network extending from ER. Cell *184*,
646 2412-2429 e2416.
647 Zhou, Y., Maxwell, K.N., Sezgin, E., Lu, M., Liang, H., Hancock, J.F., Dial, E.J., Lichtenberger, L.M., and Levental, I.
648 (2013). Bile acids modulate signaling by functional perturbation of plasma membrane domains. J Biol Chem *288*,
649 35660-35670.

650

Supplemental Information for:

Partitioning to ordered membrane domains regulates the kinetics of secretory traffic

Ivan Castello-Serrano, Fred A. Heberle, Barbara Diaz-Rohrer, Rossana Ippolito, Carolyn R. Shurer, Pablo Lujan, Felix Campelo, Kandice R. Levental, Ilya Levental

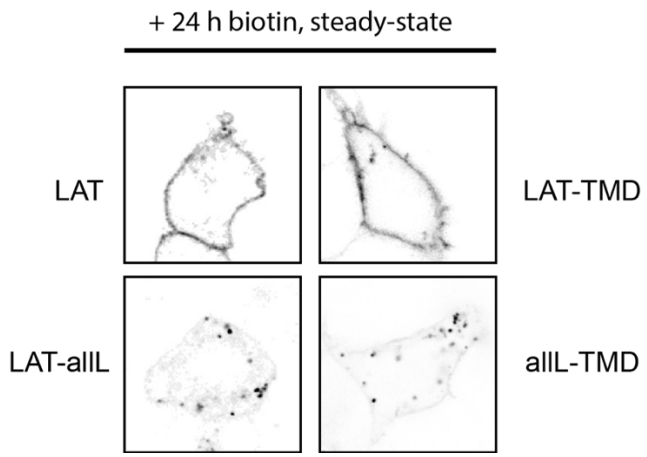

Fig S1. Representative images of RUSH constructs after overnight (>10 hours) treatment with biotin. Images show the steady-state distribution for these constructs: LAT and LAT-TMD accumulate at the PM, LAT-allL and allL-TMD accumulate in punctate structures previously identified as lysosomes.

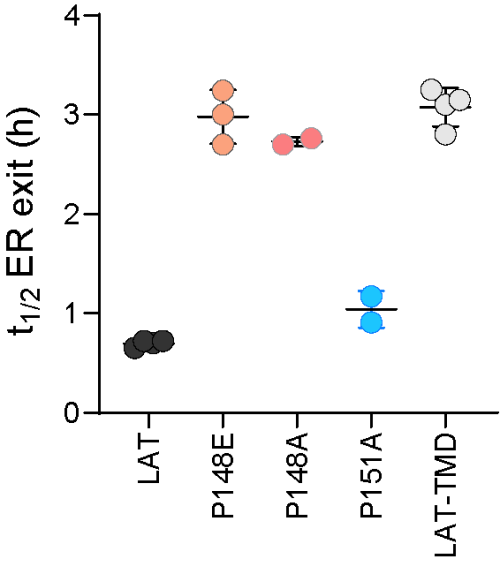

Fig S2. Half-time for ER exit for point mutations in the ΦxΦxΦ motif of LAT. P148 is critical for fast export from the ER, P151 is not.

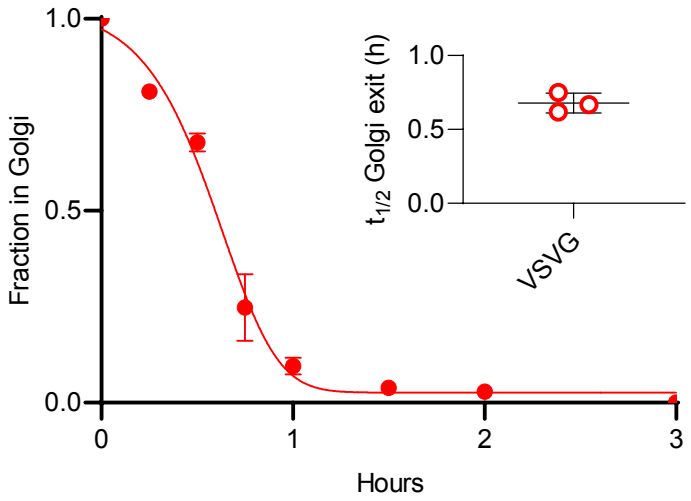

Fig S3. Fraction of RUSH-VSVG in Golgi after biotin addition. Inset represents repeats quantifications of the half-time of Golgi exit. Symbols represent average +/- st.dev. from 3 independent experiments.

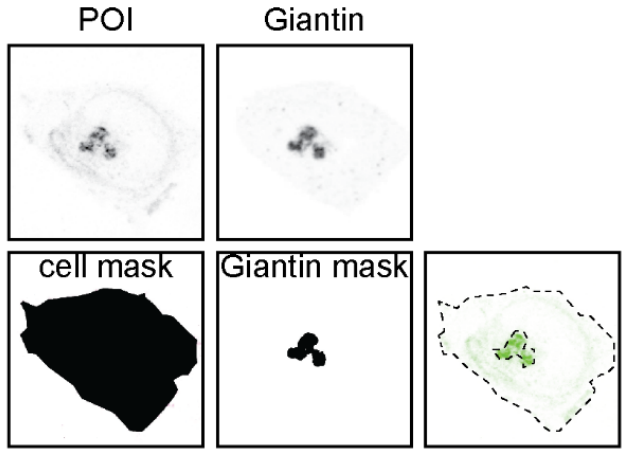

$$\text{Fraction in Golgi} = \frac{\left(\dfrac{\text{POI intensity inside giantin mask}}{\text{POI intensity inside cell mask}}\right)_{t}}{\left(\dfrac{\text{POI intensity inside giantin mask}}{\text{POI intensity inside cell mask}}\right)_{t=0}}$$

Fig S4. Example of quantification of Golgi residence for protein of interest (POI). Top panels are representative images, bottom panels are corresponding masks to calculate the fraction of POI in Golgi. Giantin was used as Golgi marker to create the mask for that organelle. Cells mask represents the cell border from the POI channel after background subtraction.

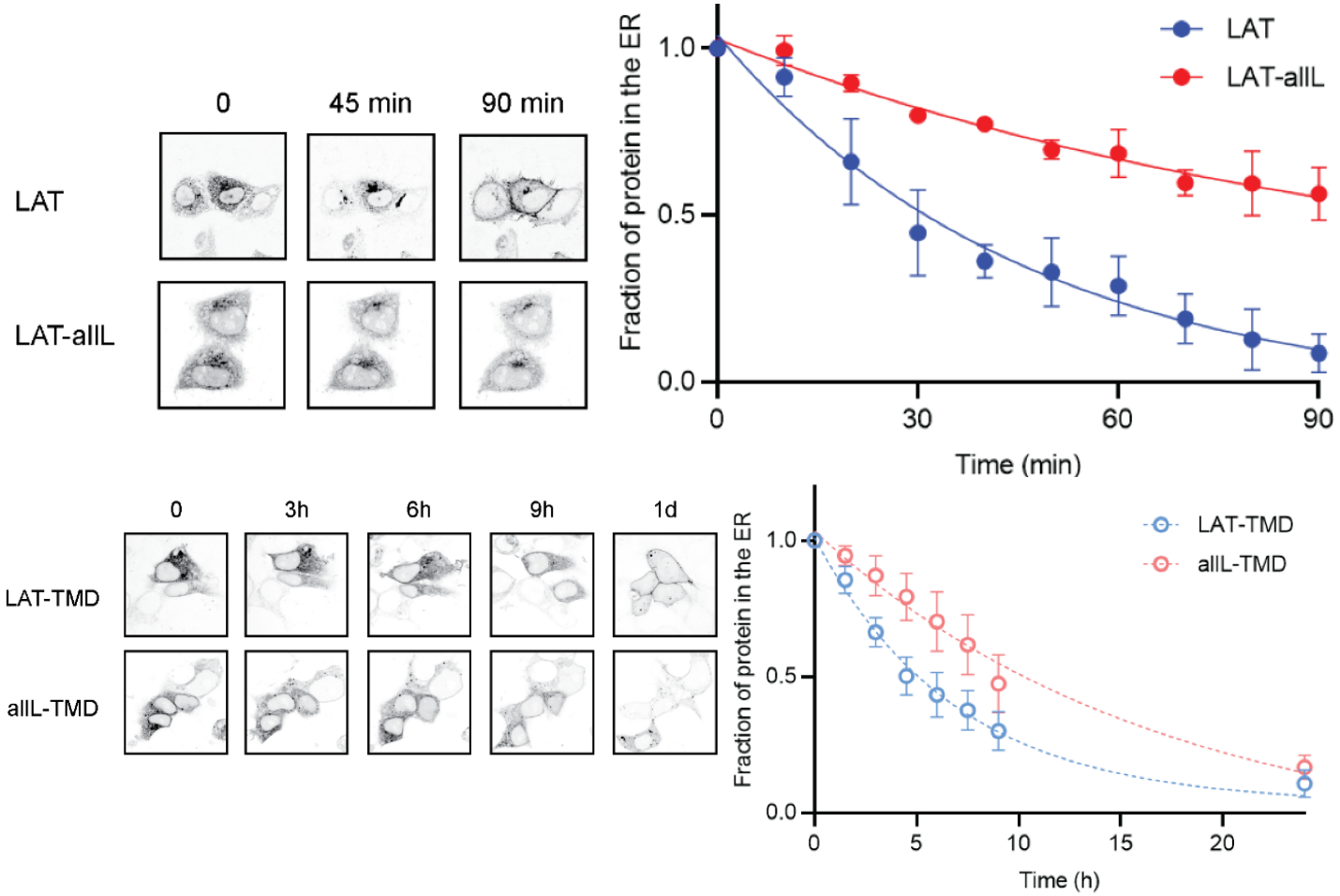

Fig S5. Representative images of the experiments measuring ER exit kinetics within individual cells, used for the kinetic modeling. Images show localization of RUSH constructs within a set of cells after biotin addition. Fraction in ER was quantified by making a mask of the protein at time 0 (i.e. before biotin addition) and calculating the remaining intensity within the mask (relative to total cellular intensity) at each subsequent time point. Top panels show full-length LAT and LAT-allL, bottom panels are LAT-TMD and allL-TMD. Symbols represent average +/- st.dev. from 3 independent experiments with multiple cells per experiment.

Table S1. Raft affinity ($K_{p,raft}$) values for constructs used in this study.

protein construct	$K_{p,raft}$ (mean±SD)
GPI	1.64 ± 0.09
LAT	1.33 ± 0.04
LAT-TMD	1.35 ± 0.06
allA8L-TMD	1.14 ± 0.13
LAT-allL	0.60 ± 0.07
allL-TMD	0.53 ± 0.01
TfR	0.37 ± 0.06
LAX	0.60 ± 0.02
LAX-TMD	0.76 ± 0.26
VSVG	0.50 ± 0.12